AIChE WILEY InterScience DISCOVER SOMETHING GREAT

MATERIALS, INTERFACES, AND ELECTROCHEMICAL PHENOMENA

Shape Evolution of 3-Dimensional Faceted Crystals

Yongchun Zhang, Jacob P. Sizemore, and Michael F. Doherty
Dept. of Chemical Engineering, University of California, Santa Barbara, CA 93106

DOI 10.1002/aic.10778
Published online February 9, 2006 in Wiley InterScience (www.interscience.wiley.com).

A novel method for modeling the shape evolution of 3-dimensional (3-D) faceted crystals has been developed in which the normal distances to each face from an origin inside the crystal are represented by a system of ordinary differential equations. The model is initialized from an arbitrary initial seed shape and size but known crystallographic data (such as unit cell and symmetry). At each time step, the entire family of possible discrete shape evolution events (such as vertices bifurcating into edges or faces, etc.) are exhaustively enumerated and investigated using a new set of simple testable conditions. The evolving crystal shape is then determined from the evolving set of normal distances and the corresponding crystallographic planes. The model has been successfully applied to two organic crystal systems: adipic acid grown from water and α-glycine grown from water. © 2006 American Institute of Chemical Engineers *AIChE J,* 52: 1906-1915, 2006
Keywords: crystallization, shape, evolution, adipic acid

Introduction

Crystals produced by solution crystallization have distinct faceted morphologies that may change during growth. Much of the crystal morphology literature is focused on the prediction of either the thermodynamic equilibrium shape or the steady-state growth shape of a crystal. These shapes are normally quite different, since the thermodynamic equilibrium shape is governed by minimizing the Gibbs free energy of each crystal, whereas the steady state growth shape is governed by the growth velocity of each crystal face. By steady state, we mean a constant trajectory of the dynamical system governing the evolution of the crystal shape; physically, this means that the crystal grows larger with a self-similar shape. Very few studies have been reported on shape evolution phenomena associated with faceted crystal growth. Among those, Prywer[1] has developed a method to predict the appearance and disappearance of faces by tracking the appearance and disappearance of each edge on the face, and has also investigated the morphology change under different operating conditions. Gadewar and Doherty[2] have developed a true dynamic model for the shape evolution of 2-D crystals with constant relative normal growth rates. By tracking the length of every edge, this model is able to describe the real-time shape evolution and to determine the steady state habit for tablet-like crystals with a dominant face. However, most crystals do not have a dominant face and cannot be approximated as 2-D.

The shape of a crystal changes along with its size during growth because in real crystallizers, the crystals may not necessarily reach their steady state shape. Moreover, the crystal nuclei, because of their different sources, can have very different sizes and shapes; therefore, even crystals with similar size can have very different shapes, none of which are at their steady states. Clearly, this has a large impact on the overall mass balance, product quality, and process design. Consequently, it is of considerable value to have a method that predicts the exact shape of a crystal grown from an arbitrary seed shape at any moment during a continuous time period under realistic operating conditions. The desired model should be able to correctly predict the major events, such as the appearance or disappearance of faces, edges, and vertices. It should also be able to predict the steady state crystal shape under a given set of operating conditions, which are not necessarily constant.

Correspondence concerning this article should be addressed to M. F. Doherty at mfd@engineering.ucsb.edu.

There is already a rich literature on dynamic models for morphology evolution of surfaces that grow geometrically. Geometric growth means that the normal velocity of the surface depends only on the position and local shape of the surface (that is, orientation). Such growth has the characteristic feature of possessing only one velocity direction at each point (i.e., forwards), in contrast to diffusion-type phenomena, which possess at least two velocity directions (forwards and backwards relative to the medium). The evolution equation for geometric growth is a first-order partial differential equation called the Hamilton-Jacobi equation, which has application to the flow of traffic on long roads[3] and water in long rivers,[4] to topography evolution in the manufacture of microelectronic devices,[5,6] and to crystal growth[7,8] (see especially the review article by Taylor, Cahn, and Handwerker[9]). Solutions to the Hamilton-Jacobi equation are capable of undergoing shock transitions, which are interpreted as transitions to faceted growth. However, for fully faceted growth morphologies, such as crystals, we propose a simpler dynamic evolution model.

The remainder of this article is organized as follows. First, the geometric fundamentals of a 3-D crystal are addressed, and a method is developed to investigate all possible shape change events. Then, the dynamic 3-D shape evolution model is developed. Finally, the model is applied to adipic acid growing in water and α-glycine growing in water.

Crystal Shape Evolution

In order to develop a model for the evolution of a crystal shape, it is necessary to describe the shape in a geometrical way. By viewing the crystal as a 3-D convex solid, we apply existing theorems of geometry to constrain the way a crystal can evolve (such as appearance of a new face) from one moment in time to the next.

Geometric fundamentals

Geometrically, a faceted crystal can be viewed as a convex 3-D solid object whose hull is surrounded by flat faces that coincide with the crystallographic planes. The crystallographic planes are dictated by the 3-D symmetry relationship(s) among the atoms/molecules in the crystal. The shape, or habit, of a crystal is commonly defined by the perpendicular distance of each face from an origin inside the crystal body. It can be equivalently defined by the area of faces, or the length of edges, or even the inter-facial angles.

A family of planes in a 3-D coordinate space can be represented by a linear equation. In the coordinate system spanned by the unit cell axes a, b, and c, a crystal face with Miller indices (hkl) is completely specified by the values of h, k, l, and m, and conveniently expressed as follows:

$$hz_1 + kz_2 + lz_3 = m \tag{1}$$

where z_1, z_2, and z_3 represent the fractional coordinates of any point satisfying Eq. 1 on the face in the given (**a**,**b**,**c**) coordinate system; m is proportional to the perpendicular distance, H, to the face from the origin; and h, k, and l define the outward normal vector to the face. For a complete discussion, we refer the reader to the Appendix. A crystal face is a finite portion of the plane defined by the above equation because of the intersection of this face with neighboring faces. With this in mind, the 3-D crystal is the convex polyhedron defined by the set of solutions to a system of linear inequalities:

$$\mathbf{Az} \leq \mathbf{M} \tag{2}$$

Each row of the $N \times 3$ matrix **A** contains the Miller indices of one face, the components of the $N \times 1$ vector **M** are the m_i for each face, **z** is the 3×1 vector of coordinates on a face, and N stands for the number of faces. The corresponding equalities denote the convex hull, that is, the faces that define the surface, or habit, of the crystal.

When studying crystal shape evolution, we will consider only the convex hull; more specifically, we will focus on the faces, edges, and vertices. For edges and vertices on the crystal surface, we note that: (i) An edge is the intersection of two faces, and (ii) A vertex is the intersection of three or more faces. It is well-known that the number of faces, edges, and vertex points, denoted as F, E, and V, respectively, for a convex polyhedron must conform to Euler's theorem for polyhedra[10]:

$$V + F - E = 2 \tag{3}$$

It is also worth noting that three or more planes can intersect on one line, forming a so-called *pencil*. However, on the surface of a polyhedron, a *pencil* cannot exist; therefore, an edge is always the intersection of two faces. A vertex point can be the intersection of three or more faces, so in order to simplify our discussion, we introduce two terms. A vertex point where exactly three faces intersect is called a *simple* vertex, while a vertex formed by n ($n>3$) faces is called an *n-compound* vertex.

Discrete morphology changes

Since crystallographic faces have different normal growth rates, the shape of a crystal changes during its growth unless the seed already has the steady state shape. Shape evolution phenomena can be divided into two categories: (i) "continuous evolution," when only changes in the relative sizes of the existing faces occur; and (ii) "structural evolution," when faces, edges, and vertices appear or disappear. Modeling continuous evolution is relatively straightforward using a set of ordinary differential equations that are described later; the major challenge is to correctly predict the discrete events that occur during structural evolution. A dynamic shape evolution model must be able to capture both kinds of evolution scenarios.

All convex polyhedra must obey Euler's theorem for polyhedra, so the condition

$$\Delta V + \Delta F - \Delta E = 0 \tag{4}$$

must always be satisfied for valid structural evolution while the crystal remains a convex polyhedron. This condition enables us to exhaustively investigate the possible structural changes that can occur.

Physically, a crystal grows by incorporating solute molecules that have finite size onto its surfaces. However, from a macroscopic point of view (particles larger than O (50-100) nm

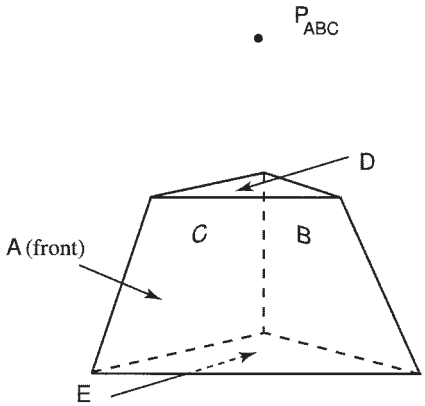

Figure 1. A 5-faced crystal with only simple vertices.

for organic systems), the molecules appear sufficiently small so that the growth can be viewed as a continuous process. As an existing face disappears, its area decreases smoothly to zero and the face eventually reduces to an edge or a vertex. On the other hand, a new face can only emerge from an existing edge or vertex, and its area smoothly increases from zero.[1] However, we show that given a set of possible crystallographic faces, in order to predict the appearance of a new face or edge for an existing crystal, we only need to investigate all the possible structural change scenarios associated with every vertex point.

For a set of $n \geq 3$ non-parallel faces, the maximum numbers of edges and vertices that may form are

$$E_{\max} = \mathcal{C}_2^n, \quad V_{\max} = \mathcal{C}_3^n \tag{5}$$

where $\mathcal{C}_m^n = n!/(n-m)!m!$ $(n \geq m)$ stands for the total possible combinations of arbitrarily choosing m objects out of a pool of n. The maximum number of edges is reached when every pair of faces intersects at a distinct edge, and the maximum number of vertices is reached when every group of three faces intersects at a distinct vertex. By substituting Eq. 5 into Eq. 3 and solving the resulting cubic equation, the only real solution is $n = 4$, which corresponds to a triangular pyramid (e.g., a tetrahedron), the simplest possible convex polyhedron. For any other number of faces ($n \geq 5$), the maximum number of edges *and* vertices cannot simultaneously exist on a convex polyhedron.

The actual number of edges and vertices will depend on the spatial orientation of the faces. Figure 1 shows a 5-faced crystal with only simple vertices where face D (top) and face E (bottom) are not necessarily parallel. According to Eq. 5, a group of four faces can form at most 6 edges and 4 vertices. The group of four faces A, B, C, and D taken together results in the maximum number of 6 edges but only 3 vertices; there is a virtual vertex P_{ABC} lying outside the convex hull. In contrast, the group of four faces B, C, D, and E taken together forms 5 edges and 2 vertices on the crystal surface. The virtual vertex P_{ABC} in Figure 1 will become a real vertex only when face D disappears (and the surface simultaneously loses edges l_{DA}, l_{DB}, and l_{DC}). Such a transition is represented in Figure 2a, and we conclude that, at simple vertices, the appearance of new edges and vertices must be accompanied by a new face.

At an n-compound vertex, where n faces intersect at one vertex point, there exist some virtual vertices and edges that can appear during a structural evolution even if no new face is about to appear. For instance, in Figure 2b, where four faces A, B, C, and E intersect at one point, the 4-compound vertex P_{ABCE} can be viewed as the combination of four simple virtual vertex points P_{ABC}, P_{ABE}, P_{ACE}, and P_{BCE}. Meanwhile, besides the four existing edges l_{AB}, l_{BC}, l_{CE}, and l_{EA}, there are two virtual edges, l_{AC} and l_{BE}. Since the number of real edges surrounding an n-compound vertex is always n, the maximum number of virtual edges associated with an n-compound vertex is

$$\tilde{E}_{\max} = \Delta E_{\max}^0 = \mathcal{C}_2^n - n \tag{6}$$

where the tilde indicates a virtual quantity. As indicated in Eq. 6, this number also denotes the upper limit on ΔE^0 after a structural evolution if no new face appears (the superscript "0" indicates that no new face appears). Meanwhile, because the number of real simple vertex points at an n-compound vertex is zero, the maximum number of virtual simple vertices associated with an n-compound vertex is

$$\tilde{V}_{\max} = \mathcal{C}_3^n \tag{7}$$

In contrast to Eq. 6, $\Delta V_{\max}^0 \neq \tilde{V}_{\max}$, because after a structural evolution where no new face appears, the compound vertex no longer exists. This must be accounted for as we track the evolution of real vertices, so we write

$$\Delta V_{\max}^0 = \mathcal{C}_3^n - 1 \tag{8}$$

For the four-compound vertex $C0$ in Figure 2b, $\tilde{E}_{\max} = \Delta E_{\max}^0 = 2$, $\tilde{V}_{\max} = 4$, and $\Delta V_{\max}^0 = 3$. Since $\Delta F = 0$, $\Delta E = \Delta V$ according to Eq. 4, so $\Delta V_{\max}^0 = 3$ is unattainable because $\Delta E_{\max}^0 = 2$ (later we show that even $\Delta E_{\max}^0 = 2$ is unattainable). Transitions $C0 \rightarrow C1$ and $C0 \rightarrow C2$ in Figure 2b show structural evolutions where one new edge and two new simple vertices appear, but no new face. Sine the compound vertex disappears, there is a net increase of one vertex as a result of the structural transition. The upper bounds on ΔE^0 and ΔV^0 in Eqs. 6 and 8 are not attained by these transitions.

On the other hand, when a new face appears, it must be accompanied with the emergence of new edges and vertices

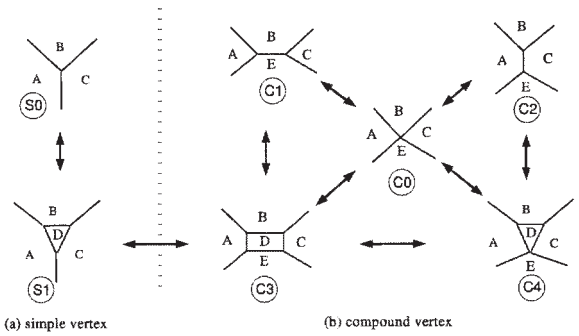

Figure 2. Structural evolution scenarios at (a) simple vertex; (b) compound vertex.

The bold arrows indicate feasible transitions.

Table 1. Shape Evolution Scenarios Associated with the Compound Vertex in Figure 2b

ΔF	ΔE & ΔV	Notes	Examples
$\Delta F = 0$	$\Delta E = \Delta V = 1$	Valid	$C0 \rightarrow C1$, $C0 \rightarrow C2$, $C3 \rightarrow C4$
$(\Delta E^0_{\max} = 2)$	$\Delta E = \Delta V = 2$	Invalid	
	$\Delta E \geq 3$	Invalid, $\Delta E^0_{\max} = 2$	
$\Delta F = 1$	$\Delta E = 1$, $\Delta V = 0$	Invalid, need $\geq$2 new edges for new face	
$(2 \leq \Delta E^1 \leq 4)$	$\Delta E = 2$, $\Delta V = 1$	Valid, face emerges from edge	$C2 \rightarrow C4$
	$\Delta E = 3$, $\Delta V = 2$	Valid, face emerges from vertex or edge	$C0 \rightarrow C4$, $C1 \rightarrow C3$, $C2 \rightarrow C3$
	$\Delta E = 4$, $\Delta V = 3$	Valid, face emerges from vertex	$C0 \rightarrow C3$
	$\Delta E \geq 5$	Invalid, $\Delta E^1_{\max} = 4$	

(when $\Delta F > 0$, $\Delta E = \Delta V = 0$ does not satisfy Eq. 4). Since one face consists of at least three edges and three vertices, the minimum number of new edges, $\Delta E^1_{\min}$, is two, denoting a triangular face emerging from an existing edge. The maximum number of new edges, $\Delta E^1_{\max}$, is n, which occurs when the new face intersects with every existing face surrounding the vertex. The maximum and minimum number of new vertices can then be obtained using Euler's theorem in Eq. 4.

With these guidelines, it is now possible to exhaustively investigate all the possible structural change phenomena during crystal growth. We illustrate the method with the example shown in Figure 2.

At a simple vertex, there is no virtual edge or vertex, so the only possible structural change is the appearance of a new triangular face cutting into all three existing faces (see Figure 2a). Figure 2b illustrates the possible structural evolution scenarios associated with a four-compound vertex point, which has a maximum number of virtual edges and vertices of two and four, respectively. When no new face appears, that is, $\Delta F = 0$ ($\Delta E^0_{\max} = 2$; $\Delta E = \Delta V$), the possible structural changes are from State $C0$ to either State $C1$ or State $C2$, corresponding to the condition $\Delta E = \Delta V = 1$. The transition from State $C4$ to State $C3$ is equivalent to that from State $C0$ to State $C1$; i.e., $\Delta F = 0$ and $\Delta E = \Delta V = 1$. If $\Delta E = 2$, both virtual edges l_{AC} and l_{BE} must appear. Consequently, all three virtual vertices must appear, i.e., $\Delta V = 3$, because these two edges do not share any vertex point. However, this contradicts Euler's theorem, which demands $\Delta V = \Delta E$ if $\Delta F = 0$. When $\Delta F = 1$, the only possible situations are $\Delta E = 2$, 3, or 4, as listed in Table 1. Table 1 is organized in the following way: ΔF is fixed, ΔE is varied from $\Delta E^{(\Delta F)}_{\min}$ to $\Delta E^{(\Delta F)}_{\max}$, and ΔV is determined by Eq. 4 for each value of ΔE.

Remark 1: State $C4$ in Figure 2 is representative of four possible shapes, where the new triangular face can have a four-compound vertex P_{ABCD}, P_{ABED}, P_{ACED}, or P_{BCED}.

Remark 2: State $C1$ cannot evolve to State $C2$ directly without taking an intermediate step, such as $C1 \rightarrow C0 \rightarrow C2$ or $C1 \rightarrow C3 \rightarrow C2$.

Remark 3: The transitions $C1 \rightarrow C3$ and $C2 \rightarrow C4$ denote the situation when a new face emerges from an edge. However, it demonstrates that this scheme is capable of predicting face appearance not only from an n-compound vertex, but also from an edge, which completes the investigation of structural evolutions.

Remark 4: Structural changes accompanied by faces, edges, and/or vertices disappearing can be viewed as the reverse of the aforementioned problem. Double-directioned arrows in Figure 2 denote the feasible transitions from one state to another.

Figure 3 shows a 3-D illustration of structural evolution phenomena associated with a four-compound vertex. Note that face B is behind face E. The structural change scenarios for an n-compound vertex when $n \geq 5$ are more complicated, but they can be worked out using the same procedure.

Dynamic Shape Evolution Model

Having developed a scheme for exhaustively listing the possible structural evolutions that can occur for a crystal, we now develop governing equations for the continuous growth of a crystal in time. As will be shown, they can be written as ordinary differential equations describing the rate of growth of the normal distances to each face from an origin inside the crystal.

Shape calculation procedure

The shape of a crystal depends on the crystallographic faces and their relative perpendicular distances from an origin inside the crystal. If the total number of faces is denoted as N, the maximum number of possible vertices is $\mathcal{C}^N_3$. The position of these vertices can be computed exhaustively from all the possible triple-face combinations. The validity of each of these computed vertices is then verified by checking against the linear inequalities in Eq. 2. All the edges on the surface can then be identified from the set of valid vertices, and the shape of the crystal is determined (see also Dowty[11]).

It is worth mentioning that for a set of crystal faces with arbitrary perpendicular distances, not all the candidate faces necessarily exist on the crystal surface, and some faces with large perpendicular distances lie outside the crystal. We term these faces *virtual* in contrast to the visually *real* faces with

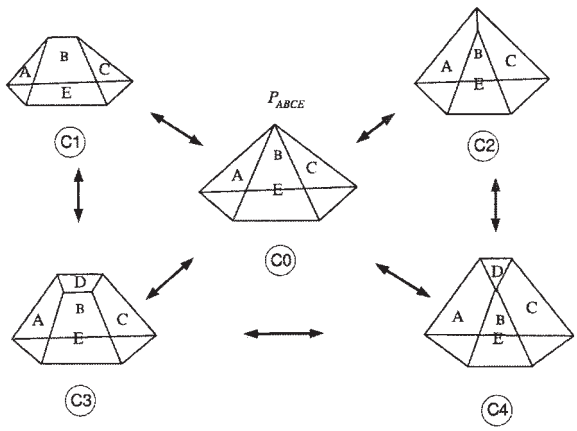

Figure 3. A 3-D view of structural evolutions at a compound vertex.

non-zero surface area. The *virtual* faces can be viewed as a degenerated face of zero area.

Different views of crystal shape evolution

As a crystal grows, all the metric quantities, such as (i) the perpendicular distances to each face from an origin, (ii) face areas, (iii) length of each edge, and (iv) spatial location of every vertex point, change; yet, each of these quantities can be used to determine the crystal shape. As there are different ways to define a crystal shape, researchers have studied crystal shape evolution from different points of view by following the change of these different metrics. Bonilla et al.[12] developed a dynamic shape evolution model for 2-dimensional crystals by tracking the spatial location of every vertex point. Gadewar and Doherty[2] developed a true dynamic shape evolution model for 2-D crystals by tracking the length of each edge (which is analogous to the area in 3-D). This model has the advantage of being able to predict not only the dynamic shape evolutions, but also a well defined steady state shape. Prywer[1] presented a method to predict the disappearance of any crystal face on a 3-dimensional crystal by tracking the length of each edge.

Theoretically, all of these methods could be extended to model the dynamic shape evolution of 3-D crystals in real time. However, none of these methods has yet offered a way to describe the complete picture of shape evolution for real 3-D crystals. A disadvantage of using Bonilla's method is that it does not present a well defined steady state solution directly from the model. The difficulty in using Prywer's method for dynamic modeling lies in the bookkeeping of all the edges. An edge is shared by two faces and calculation of the tangential (lateral) edge velocity requires the information of four surrounding faces of the given edge. Besides, it is difficult to predict the appearance of edges and faces by simply tracking the lengths of the existing edges. A 3-D dynamic model based on the extension of Gadewar's method requires calculating the rate of change of all the face areas on a 3-D crystal. However, the description of crystal shape evolution based on face areas is awkward and not aligned with typical kinetic growth models, which calculate growth rates in the normal direction to the crystal faces.

Therefore, we develop a shape evolution model that describes the temporal evolution of the perpendicular distance of all the crystal faces. As will be shown, by tracking the perpendicular distances, it is possible to predict the appearance and disappearance of crystal faces. The location and evolution of edges and vertices can be determined by the shape calculation method described in the previous section.

Dynamic model

For a system of solute and solvent, the major candidate crystallographic faces likely to appear during crystal growth and growth kinetics can be predicted using first principle models[13-16], or empirical data can be used for growth kinetics. Denote H_i and G_i as the perpendicular distance (e.g., μm) and normal growth rate (e.g., $\mu m/s$) of face i, respectively (Figure 4). The relationship between H_i and G_i is given by:

$$\frac{dH_i}{dt} = G_i \quad i = 1, \cdots, N \tag{9}$$

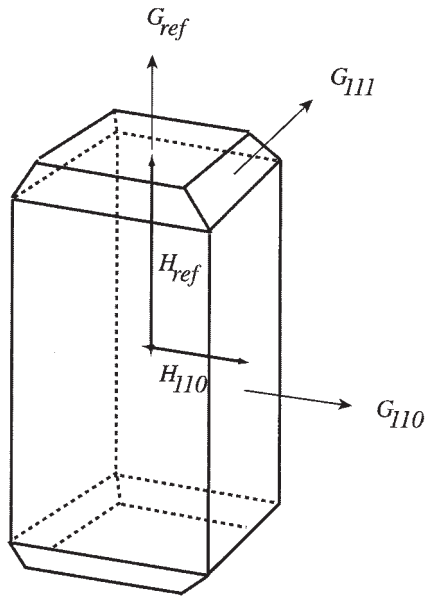

Figure 4. 3-D crystal.

This equation suffers from the disadvantage that it does not have a steady state, yet it is known that crystals growing under uniform conditions eventually evolve with self-similar shape (that is, steady state shape). This can be captured by introducing reference variables and nondimensionalizing Eq. 9. Choosing the perpendicular distance of a reference face, H_{ref}, as the characteristic length of the crystal, $G_{\text{ref}} = dH_{\text{ref}}/dt$ as the characteristic growth rate, $x_i = H_i/H_{\text{ref}}$ as the dimensionless perpendicular distance of face i, and relative growth rate $R_i = G_i/G_{\text{ref}}$, we derive a dynamic model for each crystal face:

$$\frac{dx_i}{dt} = \frac{G_{\text{ref}}}{H_{\text{ref}}}(R_i - x_i) \quad i = 1, \cdots, N-1 \tag{10}$$

$$\frac{dH_{\text{ref}}}{dt} = G_{\text{ref}} \qquad s.t. \quad h_i z_1 + k_i z_2 + l_i z_3 \le m_i(t) \tag{11}$$

where the coefficients h_i, k_i, and l_i are the Miller indices, and $m_i(t) = D_i H_i(t)$, where D_i is a constant (see Appendix).

Defining a new variable $d\xi = (G_{\text{ref}}/H_{\text{ref}})dt$, which represents a dimensionless "warped" time, Eqs. 10 and 11 can be rewritten in the dimensionless form:

$$\frac{dx_i}{d\xi} = R_i - x_i \quad i = 1, \cdots, N-1 \tag{12}$$

$$\xi = \ln\left(\frac{H_{\text{ref}}}{H_{\text{ref}}(0)}\right) \qquad s.t. \quad h_i z_1 + k_i z_2 + l_i z_3 \le m_i(\xi) \tag{13}$$

In order to ensure that the time transformation $t \rightarrow \xi$ has no time reversal, the quantity G_{ref}/H_{ref} must be positive definite and finite for all finite time. Therefore, in our model, the reference face must be chosen to be a face that never disappears (since the growth rates of real faces are never zero or infinite).

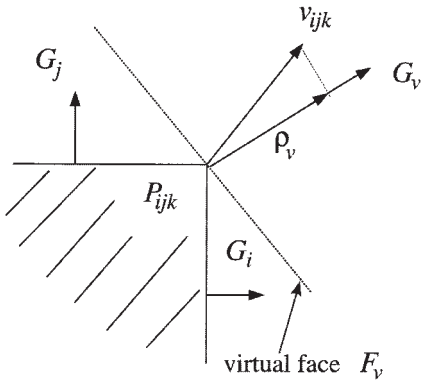

Figure 5. Appearance of a virtual face at vertex P_{ijk} (face F_k not shown).

We emphasize that this evolution model is totally independent of any physical model used to describe the growth rate of faces, as long as the previously described time transformation has no time reversal. Up to this point, the only assumption about crystal growth we have made is that the crystal is faceted for all time.

When the relative growth rates are constant, the model in Eqs. 12 and 13 is a linear system of ODEs and all the eigenvalues are equal to -1; therefore, it has a unique and stable steady state solution, given by:

$$x_i = R_i \Leftrightarrow \frac{H_i}{H_{\text{ref}}} = \frac{G_i}{G_{\text{ref}}} \quad i = 1, \cdots, N-1 \tag{14}$$

which is exactly the Chernov condition.[7]

In general, the R_i will depend on supersaturation (and possibly other quantities), which couples Eq. 12 to the mass and energy balances for the crystallizer device (especially a batch crystallizer). In such cases, the dynamics of crystal growth may not be so well-behaved as compared to the case when all R_i are constant.

It is only the ODEs corresponding to the *real* faces in the model that are integrated continuously over time. The $H_i(t)$ of the *virtual* faces are computed geometrically by assuming that they are located on the crystal surface in the degenerated form of an edge or a vertex.

Discrete events: vertex dynamics

At each instant in time, existing vertices on the crystal surface may bifurcate into other structures involving additional vertices, edges, and/or faces. The key issues are how to test when such events are about to occur and how to determine which of the allowable geometric forms emerge. This is done using a straightforward test outlined below.

Assume a virtual face F_v with Miller indices $(h_v k_v l_v)$ and normal growth rate G_v is located on the simple vertex P_{ijk} of three intersecting faces F_i, F_j, and F_k (Figure 5). The velocity vector $\mathbf{v}_{ijk}$ of this vertex point is given by:

$$\mathbf{v}_{ijk} = \begin{bmatrix} h_i & k_i & l_i \\ h_j & k_j & l_j \\ h_k & k_k & l_k \end{bmatrix}^{-1} \begin{bmatrix} G_i \\ G_j \\ G_k \end{bmatrix} \tag{15}$$

and the projection of this velocity onto the normal direction of F_v is

$$\rho_v = \frac{\mathbf{v}_{ijk}^T \mathbf{n}_v}{\|\mathbf{n}_v\|} \tag{16}$$

where $\mathbf{r}_1^T \mathbf{r}_2$ represents the inner (dot) product between vectors $\mathbf{r}_1$ and $\mathbf{r}_2$, $\|\mathbf{r}_1\|$ represents the norm of vector $\mathbf{r}_1$, and $\mathbf{n}_v$ represents the vector normal to face $(h_v k_v l_v)$ (see Appendix). In general, the velocity vectors $G_v \mathbf{n}_v$ and $\mathbf{v}_{ijk}$ will not be parallel (as seen in Figure 5), but $G_v \mathbf{n}_v$ and $\rho_v \mathbf{n}_v$ are parallel, so their magnitudes (speeds) can be directly compared.

Face F_v will appear if $\rho_v > G_v$, because it is moving slower than the vertex. Therefore, the virtual face becomes a real face on the crystal surface and intersects the other existing faces at vertex point P_{ijk}. When $\rho_v \leq G_v$, face F_v will remain virtual. For degenerated faces in the form of an edge on the surface, the foregoing criterion is still valid because the velocity vector of either end point can be used in the comparison. We can summarize these observations as follows:

$$\rho_v \leq G_v \Rightarrow F_v \text{ remains virtual} \qquad \rho_v > G_v \Rightarrow F_v \text{ appears} \tag{17}$$

We test for the splitting of an n-compound vertex in a similar way. Consider the case of a four-compound vertex consisting of faces A, B, C, and E intersecting at a single point. By computing the velocity vectors of the virtual vertices $\mathbf{v}_{ABC}$, $\mathbf{v}_{ABE}$, $\mathbf{v}_{ACE}$, and $\mathbf{v}_{BCE}$, we determine which, if any, of the discrete events represented in Figure 2b occur. For example, if $\mathbf{v}_{ABE} = \mathbf{v}_{BCE}$ and if $\mathbf{v}_{ACE}$ points away from $\mathbf{v}_{ABC}$, then edge l_{BE} will form, corresponding to the transition $C0 \rightarrow C2$ in Figure 2b. In addition, the instant edge l_{BE} forms, all the virtual vertices are eliminated and only *real* vertices ACE and ABC remain. A special case occurs if the velocity vectors for the virtual vertices are collinear and of equal magnitude: in this case, the four-compound vertex persists and no discrete events take place at this vertex.

Now we are able to solve the dynamic model continuously over the time horizon. The computational procedure for solving this model for general operating conditions is summarized as follows:

(1) Start from an arbitrary given initial condition of polymorph, seed size and shape, and allowable crystallographic planes. Perform a shape calculation, identify the real and virtual faces, and calculate all the dimensionless perpendicular distances $x_i(\xi)$ at time $\xi = 0$.

(2) Determine the virtual faces that are about to become real.

(3) Integrate the set of ODEs representing all the real faces and all the virtual faces that are about to become real over a small step $\Delta\xi$. At the end of the step, perform a shape calculation to verify the validity of these faces. Calculate the x_i for the virtual faces that were not involved in the integration.

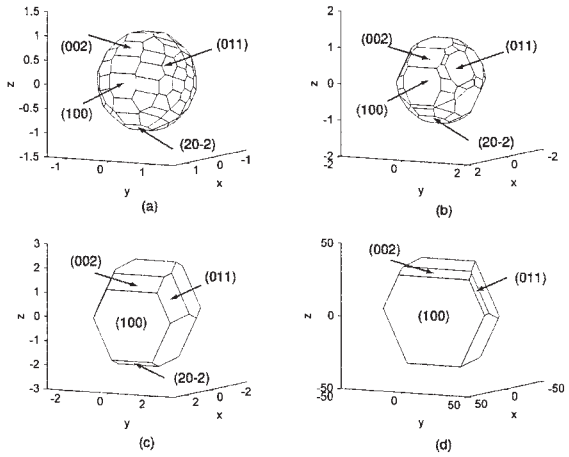

Figure 6. Evolution of adipic acid ($\Delta\xi = 0.025$).

(a) Seed ($\xi = 0$), (b) $\xi = 0.025$, (c) $\xi = 0.25$, (d) Steady state ($\xi \rightarrow \infty$).

(4) Repeat Steps 2 and 3 until the end of the batch crystallization.

Application of Model

Two systems, adipic acid and α-glycine, each grown from water, are used to demonstrate certain features of the model, as well as its general efficacy in predicting the evolution of shape over time. We simulate the shape evolution from a "spheroidal" seed, which is generated by determining a large number of faces that are allowed under the given symmetry constraints and unit cell parameters of the system. For both examples in this work, we initialized the evolution with roughly 100 faces, although there is no difficulty in selecting a larger or smaller set of faces. The entire set of faces initially is assigned an equal distance from the center, yielding a spheroid. The high-index faces are given large relative growth rates ($R = 10$), since we assume they will not appear in the steady state shape. Since many time-dependent population balance models employ spherical seeds or nuclei that evolve axisymetrically, we can use our non-axisymmetric evolution model to estimate the error (in terms of uptake of mass, actual crystal size and shape, etc.) in the axisymmetric evolution approximation for faceted crystals.

Adipic acid

Adipic acid grown from water tends to be lozenge-shaped with large {100} forms. Its unit cell parameters[17] are $a = 10.10$ Å, $b = 5.15$ Å, $c = 10.06$ Å, and $\beta = 136.45°$, and its space group is $P2_1/c$. We have followed the method of Winn and Doherty[14] to determine likely faces and calculate their perpendicular growth rates. The likely forms are {100}, {10$\bar{2}$}, {20$\bar{2}$}, {11$\bar{1}$}, and {011}. For these forms, we calculated the relative growth rates to be 1.00, 3.04, 4.80, 3.61, and 3.69, respectively. The simulated conditions of growth (T, supersaturation) were such that the expected mechanism of growth is by spirals from screw dislocations.

The essential steps involved in calculating the *ab initio* relative normal face growth rates are the following: (1) Obtain the geometry of the solute molecule. This entails gathering data on the crystal unit cell and space group, and also data on the 3-D coordinates of the atoms of the molecule. (2) Assign charges to the atoms. This can be performed with any number of electronic structure calculation packages. (3) Calculate the intermolecular interactions in the solid. This is done by building up the crystal with the geometry, then using an appropriate model of interatomic interactions together with the charge data. (4) Use the intermolecular interactions and the geometry data to determine the periodic bond chains (PBCs). (5) Apply the Bravais-Friedel-Donnay-Harker method to determine a superset of crystallographic planes allowed under the crystal space group's extinction conditions. (6) Use the PBCs and the set of crystallographic planes to determine which planes contain two or more non-parallel PBCs, which planes contain exactly one PBC, and which planes contain zero PBCs. (7) Determine the effect of the solvent on the energetics of the crystal surfaces and the prevailing growth mechanism. This discussion is too detailed to be given here, so we refer the reader to Winn and Doherty[14] or Bisker-Lieb and Doherty.[15] However, we point out that these methods yield constant relative growth rates that satisfy the conditions that lead to Eq. 14. When the evolution model is initialized with the list of crystallographic planes from Step 5 and their corresponding relative normal growth rates, the steady-state shape is an *output* of the evolution calculation.

The results of the simulated evolution are shown in Figures 6 and 7. The instantaneous shape of adipic acid at different times is shown in Figure 6, while the dimensionless perpendicular distance of selected faces is shown in Figure 7 (the distance H_{hkl} is normalized by the distance of the reference face, (100), which is why x_{100} is always 1). In Figure 6, ξ is a dimensionless time based on the reference face's growth rate and normal distance from the origin; $\Delta\xi$ is the increment in dimensionless time used in the integration scheme for Eq. 12; in this case, $\Delta\xi = 0.025$. The number of time steps n is given by $\xi/\Delta\xi$.

We are able to track the progress of a particular face toward steady state by simultaneously plotting the dimensionless perpendicular distance $x_{hkl} = H_{hkl}/H_{ref}$ (the solid lines in Figures

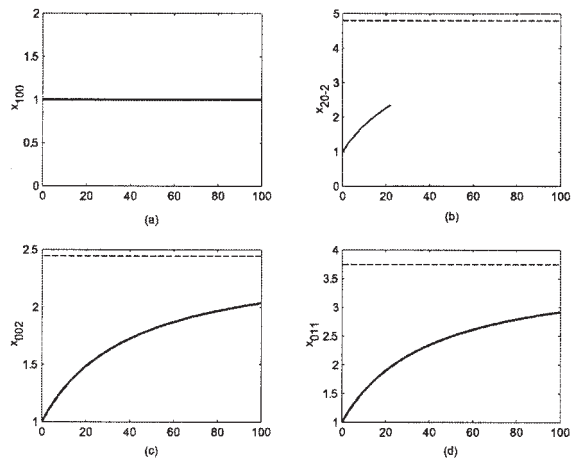

Figure 7. Time evolution of dimensionless distances for selected faces on adipic acid ($\xi_{max} = 2.5$, $\Delta\xi = 0.025$).

(a) (100), (b) ((20$\bar{2}$) disappears at n = 23, (c) (002), (d) (011) (dashed line indicates value of relative growth rate).

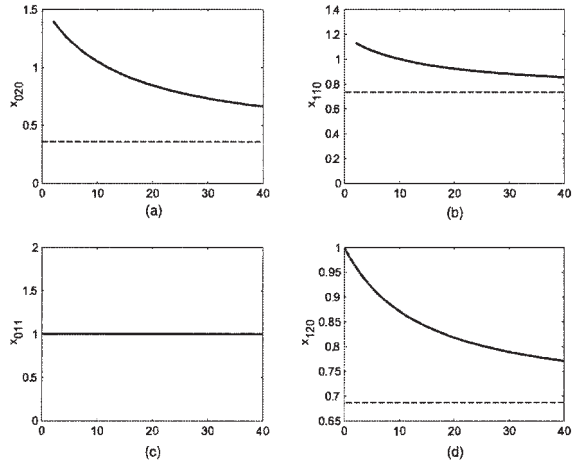

Figure 8. Time evolution of dimensionless distances for α-glycine (ξ_{max} = 1.0, $\Delta\xi$ = 0.025).

(a) (020), (b) (110), (c) (011), (d) (120) (dashed line indicates value of relative growth rates).

7 and 8) and the relative growth rate $R_{hkl} = G_{hkl}/G_{ref}$ (the dashed lines in Figures 7 and 8).

One important feature of the shape evolution model is that it accounts for the discrete event of face disappearance. In the case of adipic acid, $\{20\bar{2}\}$ is such a face. In Figures 6a-6c, $\{20\bar{2}\}$ is present, but has disappeared by the time the crystal reaches its steady state shape. There is an important distinction to be made here: the perpendicular distance of $\{20\bar{2}\}$ from the origin does not become zero when the face disappears from the crystal surface, even though the area of the $\{20\bar{2}\}$ face does become zero. This is because the virtual edge behind it "grows in" according to the condition in Eq. 17.

We have grown adipic acid from water using a saturation temperature of 25.0°C and a supersaturation of $(C - C_{sat})/C_{sat} \simeq 0.05$ (corresponding to a temperature of 24.0°C) in a seeded batch crystallizer over 40 hrs. The resulting growth shape is shown in Figure 9, which compares well with the predicted steady state shape in Figure 6d. For a description of the crystallization apparatus, see the work of Gadewar et al.[18]

α-glycine

At steady state, the α polymorph of glycine grown from water displays a coffin shape crystal bound by the {020} forms.

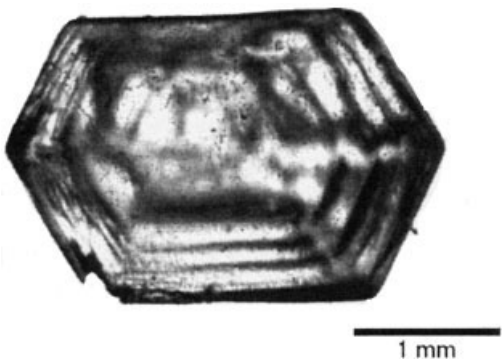

Figure 9. Shape of adipic acid grown from water.

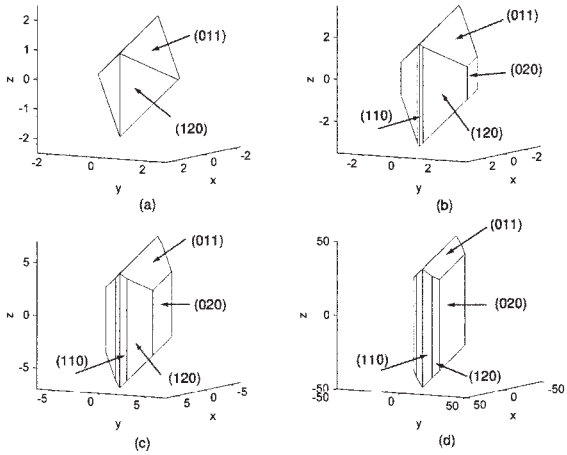

Figure 10. Evolution of α-glycine ($\Delta\xi$ = 0.025).

(a) Seed (ξ = 0), (b) ξ = 0.25, (c) ξ = 1.0, (d) Steady state ($\xi \to \infty$).

Its unit cell parameters[19] are a = 5.1054 Å, b = 11.9688 Å, c = 5.4645 Å, and β = 111.697°, and its space group is $P2_1/n$. Following the work of Bisker-Leib and Doherty,[15] we determined the likely faces to be {020}, {011}, {110}, $\{10\bar{1}\}$, $\{11\bar{1}\}$, $\{02\bar{1}\}$, and {120}, with relative growth rates of 1.00, 2.62, 2.10, 10, 10, 2.84, and 1.96, respectively. A relative growth rate of 10 is given to faces that have large interplanar spacing d_{hkl} but no strong periodic bond chains.[7] Once again, the dominant mechanism of growth is via the screw dislocation mechanism.

We have simulated the shape of α-glycine starting from a spheroidal seed, and the results are similar to those of adipic acid, whereby the faceted shape emerges out of the spheroidal initial condition. A more interesting case, however, is the evolution of α-glycine from a diamond-shaped seed containing the {120} and {011} forms. The results of such a simulation are shown in Figures 10 and 8. These figures clearly show that the model can also account for the discrete event of face appearance. In Figure 10a the {020} and {110} forms are absent from the seed, yet appear at the beginning of the simulation; ultimately, {020} becomes the dominant form. The steady state shape compares well with the experimental growth shape determined by Boek et al.[20]

Conclusions

A model has been developed that can predict the evolution of a crystal of known polymorphic form from an arbitrary seed shape. The model accounts for the continuous process of growth as well as the discrete geometric events associated with growth (e.g., edges bifurcating into faces, vertices bifurcating into edges), and it is general enough to account for time-varying or state-varying growth rates. The model requires knowledge of the unit cell and symmetry data, as well as the likely crystallographic faces and their associated growth rates. The model was applied to predict the shape evolution of adipic acid grown from water and α-glycine grown from water. The predicted steady state shapes agree well with measurements.

The shape evolution predictions we have made could be measured experimentally in several different ways. One method would be to use a single-crystal growth apparatus

coupled with video microscopy,[21] while another would be a closed cell apparatus coupled to an optical microscope.[22] A third possibility is the use of a fluidized crystallizer.[18] The advantage of the first two methods is that measurement of shape occurs *in situ*, while the third method requires the periodic removal of the crystal from the supersaturated solution. The main advantage of the third method is that the growing crystal is isolated from the vessel walls, so that kinetic growth models are greatly simplified.

Acknowledgments

We are grateful for financial support provided by Rhodia and the National Science Foundation (Grant No. CTS-0411630). In addition, this work was partially supported by the MRSEC Program of the National Science Foundation under Award No. DMR00–80034. We acknowledge helpful suggestions from Philippe Carvin of Rhodia Central Research Department.

Literature Cited

1. Prywer J. Three-dimensional model of any shape face disappearance in crystal habit. *J Cryst Growth.* 1996;158:568-575.
2. Gadewar S, Doherty MF. A dynamic model for evolution of crystal shape. *J Cryst Growth.* 2004;267:239-250.
3. Lighthill MJ, Whitham GB. On kinematic waves. 2. A theory of traffic flow on long crowded roads. *Proc Roy Soc.* 1955;229:317-345.
4. Lighthill MJ, Whitham GB. On kinematic waves. 1. Flood movement in long rivers. *Proc Roy Soc.* 1955;229:281-316.
5. Cooperberg DJ, Vahedi V, Gottscho RA. Semiempirical profile simulation of aluminum etching in Cl-2/BCl3 plasma. *J Vac Sci Technol A.* 2002;20:1536-1556.
6. Hamaguchi S, Dalvie M. Microprofile simulations for plasma-etching with surface passivation. *J Vac Sci Technol A.* 1994;12:2745-2753.
7. Chernov AA. The kinetics of the growth forms of crystals. *Sov Phys Cryst USSR.* 1963;7:728-730.
8. Frank FC. On the kinematic theory of crystal growth and dissolution processes. In: Doremus RH, Roberts BW, Turnbull D. *Growth and Perfection of Crystals*. New York: John Wiley & Sons, Inc., 1958: 411-419.
9. Taylor JE, Cahn JW, Handwerker CA. Geometric models of crystal growth. *Acta Metall Mater.* 1992;40:1443-1474.
10. Courant R, Robbins H. Topology. In: Newman, JR. *The World of Mathematics Vol. 1*. New York: Simon & Schuster, 1956:581-599.
11. Dowty E. Computing and drawing crystal shapes. *Amer Mineral Chem.* 1980;65:465-471.
12. Bonilla G, Vlachos DG, Tsapatsis M. Simulations and experiments on the growth and microstructure of zeolite MFI films and membranes made by secondary growth. *Microporous and Mesoporous Mater.* 2001;42:191-203.
13. Hartman P, Perdok PG. On the relations between structure and morphology of crystals. I *Acta Cryst.* 1955;8:49-52.
14. Winn D, Doherty MF. A new technique for predicting the shape of solution-grown organic crystals. *AIChE J.* 1998;44:2501-2514.
15. Bisker-Leib V, Doherty MF. Modeling crystal shape of polar organic materials: applications to amino acids. *Cryst Growth Des.* 2003;3:221-237.
16. Liu XY, Boek ES, Briels WJ, Bennema P. Prediction of crystal growth morphology based on structural analysis of the solid-fluid interface. *Nature.* 1995;374:342-345.
17. Housty J, Hospital M. Localisation des atomes d'hydrogene dans l'acide adipique $COOH[CH_2]_4COOH$. *Acta Cryst.* 1965;18:693-697.
18. Gadewar SB, Hofmann HM, Doherty MF. Evolution of crystal shape. *Cryst Growth Des.* 2004;4:109-112.
19. Jönsson P, Kvick Å. Precision neutron diffraction structure determination of protein and nucleic acid components. III. The crystal and molecular structure of the amino acid α-glycine. *Acta Cryst B.* 1972; 28:1827-1833.
20. Boek ES, Feil D, Briels WL, Bennema P. From wave function to crystal morphology: application to urea and alpha-glycine. *J Cryst Growth.* 1991;114:389-410.
21. Kind M, Mersmann A. On supersaturation during mass crystallization from solution. *Chem Eng Technol.* 1990;13:50-62.
22. Veesler S, Ferte N, Costes M, Czjzek M, Asteir J. Temperature and pH effect on the polymorphism of aprotinin (BPTI) in sodium bromide solutions. *Cryst Growth Des.* 2004;4:1177-1141.
23. Weisstein EW. Plane. From MathWorld—A Wolfram Web Resource. http://mathworld.wolfram.com/Plane.html.
24. Giacovazzo C. Crystallographic computing. In: Giacovazzo, C, ed. *Fundamentals of Crystallography*. New York: Oxford University Press, Inc., 1992:61-140.

Appendix: Calculations in Crystallography

Calculations involving vectors, distances, and angles are generally simpler to perform and easier to visualize in a Cartesian coordinate system as opposed to a coordinate system defined by the magnitude and direction of a crystal's unit cell axes, which may not be mutually perpendicular. Since the model we have developed requires many of these calculations, we include the material in this appendix.

Representing points in different coordinate systems

Let $\mathbf{e}_1$, $\mathbf{e}_2$, and $\mathbf{e}_3$ be orthonormal basis vectors in a Cartesian coordinate system, expressed in terms of the canonical basis vectors $(100)^T$, $(010)^T$, and $(001)^T$. Any point in the space (X_1,X_2,X_3) can be expressed as a 3-tuple vector:

$$\mathbf{r} = X_1\mathbf{e_1} + X_2\mathbf{e_2} + X_3\mathbf{e_3} = (\mathbf{e_1e_2e_3})\begin{pmatrix} X_1 \\ X_2 \\ X_3 \end{pmatrix} = \mathbf{E}\mathbf{v_x} \qquad \text{(A1)}$$

where $\mathbf{E}$ is the orthogonal matrix ($\mathbf{E}^T = \mathbf{E}^{-1}$) of the basis vectors and $\mathbf{v}_x$ is the representation of the point in the Cartesian coordinate system. The X_i have units of length because the basis vectors have been normalized.

In a crystal system, the basis vectors are normally chosen to be the crystallographic axes **a**, **b**, and **c**. A point (z_1,z_2,z_3), where the z_i are fractional, dimensionless quantities, is usually written in this coordinate system as follows:

$$\mathbf{r} = z_1\mathbf{a} + z_2\mathbf{b} + z_3\mathbf{c} = (\mathbf{abc})\begin{pmatrix} z_1 \\ z_2 \\ z_3 \end{pmatrix} = \mathbf{A}\mathbf{v_z} \qquad \text{(A2)}$$

Meanwhile, we know that the crystallographic axes can be expressed in the Cartesian coordinate system as

$$(\mathbf{abc}) = (\mathbf{e_1e_2e_3})\begin{pmatrix} t_{1_1} & t_{1_2} & t_{1_3} \\ t_{2_1} & t_{2_2} & t_{2_3} \\ t_{3_1} & t_{3_2} & t_{3_3} \end{pmatrix} = \mathbf{ET} \qquad \text{(A3)}$$

where $\mathbf{T}(= \mathbf{E}^{-1}\mathbf{A})$ is the coordinate transformation matrix *defined* by Eq. A3 and chosen so that the origins of both coordinate systems coincide. If the columns of $\mathbf{E}$ are chosen to be the canonical basis vectors (that is, $\mathbf{E} = \mathbf{I}$), then $\mathbf{T} = \mathbf{A}$. By equating Eqs. A1 and A2, the relationship between the different coordinate systems is given by:

$$\mathbf{r} = \mathbf{E}\mathbf{v_x} = \mathbf{A}\mathbf{v_z} \qquad \text{(A4)}$$

Consequently, we have

$$\mathbf{v_x} = \mathbf{T}\mathbf{v_z} \tag{A5}$$

or equivalently

$$\mathbf{v_z} = \mathbf{T}^{-1}\mathbf{v_x} \tag{A6}$$

Representing planes in different coordinate systems

As part of the crystal growth model we employ, it is necessary to determine likely crystallographic faces ($h_ik_il_i$) in terms of the crystallographic basis vectors. Once all the ($h_ik_il_i$) are determined, we transform the description of the crystallographic faces into Cartesian coordinates in order to perform our calculations and visualize the crystal's convex hull.

The equation of a plane[23] in any coordinate system is given in terms of the normal $\mathbf{n}$ to the plane and a point $\mathbf{z}^\circ$ in the plane: $\mathbf{n}^T(\mathbf{z} - \mathbf{z}^\circ) = 0$. In terms of the crystallographic basis vectors $\mathbf{a}$, $\mathbf{b}$, and $\mathbf{c}$, the normal to a plane is given by $\mathbf{n_z} = n_{z_1}\mathbf{a} + n_{z_2}\mathbf{b} + n_{z_3}\mathbf{c}$ while $\mathbf{z} = z_1\mathbf{a} + z_2\mathbf{b} + z_3\mathbf{c}$. Inserting the expressions for $\mathbf{n_z}$ and $\mathbf{z}$ into the equation of a plane, expanding the inner product, and collecting coefficients of z_i, we obtain:

$$\begin{aligned}(n_{z_1}\mathbf{a}^T\mathbf{a} + n_{z_2}\mathbf{a}^T\mathbf{b} + n_{z_3}\mathbf{a}^T\mathbf{c})z_1 + (n_{z_1}\mathbf{a}^T\mathbf{b} + n_{z_2}\mathbf{b}^T\mathbf{b} + n_{z_3}\mathbf{b}^T\mathbf{c})z_2 \\ + (n_{z_1}\mathbf{a}^T\mathbf{c} + n_{z_2}\mathbf{b}^T\mathbf{c} + n_{z_3}\mathbf{c}^T\mathbf{c})z_3 = (n_{z_1}\mathbf{a}^T\mathbf{a} + n_{z_2}\mathbf{a}^T\mathbf{b} + n_{z_3}\mathbf{a}^T\mathbf{c})z_1^\circ \\ + (n_{z_1}\mathbf{a}^T\mathbf{b} + n_{z_2}\mathbf{b}^T\mathbf{b} + n_{z_3}\mathbf{b}^T\mathbf{c})z_2^\circ + (n_{z_1}\mathbf{a}^T\mathbf{c} + n_{z_2}\mathbf{b}^T\mathbf{c} + n_{z_3}\mathbf{c}^T\mathbf{c})z_3^\circ\end{aligned} \tag{A7}$$

The lefthand side of Eq. A7 can be identified with the left-hand side of Eq. 1, and the coefficients of z_1, z_2, and z_3 in Eq. A7 can be equated with h, k, and l, respectively. Therefore, the normal $\mathbf{n}_z$ to the crystallographic plane hkl is determined by solving the following matrix equation:

$$\begin{pmatrix}\mathbf{a}^T\mathbf{a} & \mathbf{a}^T\mathbf{b} & \mathbf{a}^T\mathbf{c} \\ \mathbf{a}^T\mathbf{b} & \mathbf{b}^T\mathbf{b} & \mathbf{b}^T\mathbf{c} \\ \mathbf{a}^T\mathbf{c} & \mathbf{b}^T\mathbf{c} & \mathbf{c}^T\mathbf{c}\end{pmatrix}\begin{pmatrix}n_{z_1} \\ n_{z_2} \\ n_{z_3}\end{pmatrix} = \mathbf{M}\mathbf{n_z} = \begin{pmatrix}h \\ k \\ l\end{pmatrix} \tag{A8}$$

where $\mathbf{M}$ is the metric tensor[24] whose elements describe the moduli of a, b, and c and the angles between them, and $\mathbf{M}^{-1}$ is the metric tensor for the reciprocal lattice. From the form of $\mathbf{M}$, it is clear that $\mathbf{M} = \mathbf{A}^T\mathbf{A}$ and $\mathbf{M} = \mathbf{M}^T$. It can be shown[24] that $\det(\mathbf{M}) = V_c^2$, where V_c is the unit cell volume, so $\det(\mathbf{M}) \geq 0$ and $\mathbf{M}$ is never singular, which means that for a given set of h, k, and l, there is a unique solution for $\mathbf{n_z}$. Once $\mathbf{n_z}$ is obtained from Eq. A8, the transformation defined in Eq. A3 is used to determine the normal $\mathbf{n_x}$ to the crystallographic plane in Cartesian coordinates, because the orientation of the plane with respect to the normal must remain the same regardless of the basis vectors (see Figure A1).

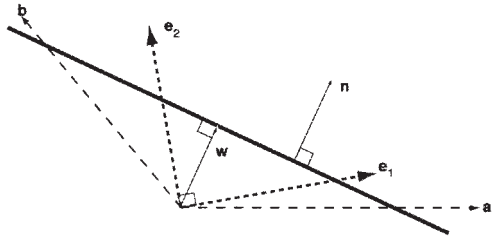

Figure A1. A 2-dimensional plane in two different coordinate bases.

Having calculated $\mathbf{n}_z$, we can now relate m in Eq. 1 with the perpendicular distance from the crystallographic plane to the origin. We construct a vector $\mathbf{w}$ (see Figure A1) that is perpendicular to the plane and starts at the origin; $\mathbf{w}$ can be equivalently expressed as $\mathbf{w_z} = (z_1 - 0)\mathbf{a} + (z_2 - 0)\mathbf{b} + (z_3 - 0)\mathbf{c}$ or $\mathbf{w_x} = (X_1 - 0)\mathbf{e_1} + (X_2 - 0)\mathbf{e_2} + (X_3 - 0)\mathbf{e_3}$. The perpendicularity of $\mathbf{w_z}$ with the plane is guaranteed by demanding that $\mathbf{w_z}$ has the following property:

$$\mathbf{n_z}^T\mathbf{w_z} = \|\mathbf{n_z}\|\,\|\mathbf{w_z}\| \tag{A9}$$

i.e., the cosine of the angle between $\mathbf{n_z}$ and $\boldsymbol{w}_z$ is unity.

If we set $\|\mathbf{w_z}\| = H$, then

$$\begin{aligned}H = \frac{\mathbf{n_z}^T\mathbf{w_z}}{\|\mathbf{n_z}\|} = (\|\mathbf{n_z}\|)^{-1}(\mathbf{A}\mathbf{n_z})^T\mathbf{A}\mathbf{z} = (\|\mathbf{n_z}\|)^{-1}\mathbf{n_z}^T\mathbf{A}^T\mathbf{A}\mathbf{z} \\ = (\|\mathbf{n_z}\|)^{-1}\mathbf{n_z}^T\mathbf{M}\mathbf{z} = (\|\mathbf{n_z}\|)^{-1}(\mathbf{M}^T\mathbf{n_z})^T\mathbf{z} = (\|\mathbf{n_z}\|)^{-1}(\mathbf{M}\mathbf{n_z})^T\mathbf{z} \\ = (\|\mathbf{n_z}\|)^{-1}(hz_1 + kz_2 + lz_3) \quad \text{by Eq. 25}\end{aligned} \tag{A10}$$

$$= \frac{m}{\|\mathbf{n_z}\|} \quad \text{by Eq. 1} \tag{A11}$$

In a Cartesian coordinate system, the generic equation for a plane can be written as $pX_1 + qX_2 + rX_3 = pX_1^\circ + qX_2^\circ + rX_3^\circ = d$. By writing out the Cartesian normal $\mathbf{n_x}$ in terms of its components, expanding the inner product $\mathbf{n_x}^T\mathbf{w_x}$, and recognizing that $\|\mathbf{w_z}\| = \|\mathbf{w_x}\|$, it is possible to show that $H = d/\|\mathbf{n_x}\|$, where $\|\mathbf{n_x}\| = \sqrt{p^2 + q^2 + r^2}$.

Manuscript received Jun 3, 2005, and revision received Dec. 8, 2005.